Inorganic Chemistry

Article

pubs.acs.org/IC

Photophysical Properties of Substituted Homoleptic and Heteroleptic Phenylimidazolinato Ir(III) Complexes as a Blue Phosphorescent Material

Takashi Karatsu,* Masatomo Takahashi, Shiki Yagai, and Akihide Kitamura

Department of Applied Chemistry and Biotechnology, Graduate School of Engineering, Chiba University, 1-33 Yayoi-cho, Inage-ku, Chiba 263-8522, Japan

Supporting Information

ABSTRACT: Iridium complexes are one of the most important materials for fabrication of organic light emitting diodes (OLEDs). There are difficulties in the preparation of blue phosphorescent complexes with respect to chromaticity, emission efficiency, and stability of the material, compared with green and red phosphorescent complexes. Control of the frontier orbital energy level (HOMO−LUMO) is the sole method to achieve better blue phosphorescent iridium complexes by appropriate ligand selection and the introduction of adequate substituents. Homoleptic and heteroleptic iridium(III) tris(phenylimidazolinate) complexes were synthesized, and the effect of the substituents on their nature in the excited state was examined. Density functional theory calculation showed that the imidazolinato complexes have the HOMO localized at the iridium d- and phenyl π-orbitals. The LUMO is also localized on the phenyl moiety with a much higher population than HOMO. This LUMO is quite different from other complexes, such as iridium(III) tris(phenylpyridinate) and tris(phenylpyrazolinate) complexes. Therefore, substitution with π-electron donating groups and electron withdrawing groups induces blue and red spectral shifts, respectively, which is the reverse shift exhibited by other complexes. The ancillary ligand (acetylacetone) acts as a path for nonradiative deactivation in the blue phosphorescent complexes.

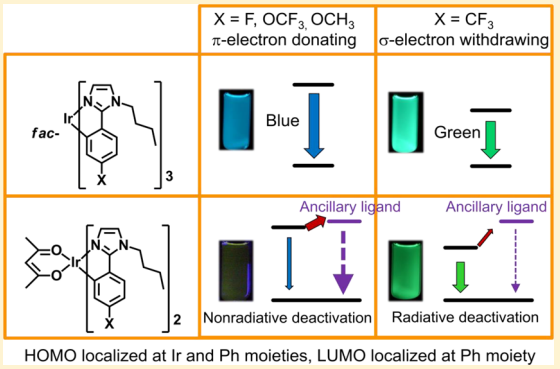

HOMO localized at Ir and Ph moieties, LUMO localized at Ph moiety

1. INTRODUCTION

Iridium complexes have a wide range of applications: in particular, the organic light emitting diode (OLED) is one of important industrial applications due to its high phosphorescent efficiency at ambient temperature.[1,2] Emitting material of OLEDs was changed from fluorescent complexes,[3,4] to phosphorescent materials such as *fac*-tris(2-phenylpyridyl)-iridium(III) (*fac*-Ir(ppy)$_3$).[5] The external efficiencies of the OLED device were increased from 1% to 7.5% during this change. These reports boosted the research activity in this field. The efficiency was jumped up to 29%, also using *fac*-Ir(ppy)$_3$, as reported by Kido and co-workers,[6] which meant an internal emission quantum yield that reached 100%. Here, not only triplet excitons (75%) but also singlet excitons (25%) were used after intersystem crossing.

Red and green phosphorescent iridium complexes have been used in commercial devices.[1] However, there are three main difficulties associated with the development of blue phosphorescent OLEDs, which are the barrier to achieve full color total phosphorescent OLED display and some types of white color lighting. The first is that they do not have sufficient color purity. The National Television Standards Committee (NTSC) determined that the Commission Internationale de l'Eclairage (CIE) coordinates for blue are (x, y = 0.14, 0.08). However, in typical blue phosphorescent complexes, such as iridium(III) bis(4,6-difluorophenylpyridinato)picolinate (FIrpic),[7] and other iridium complexes,[8,9] the sum of the x, y coordinates is more than 0.3, and the color is called sky blue. The second difficulty is insufficient emission efficiency. A blue phosphorescent complex has a higher energy emission state (^{3}MLCT, metal-to-ligand charge-transfer) than other color complexes, due to the large transition energy. This enables thermal activation to the metal-centered excited state (d*), which promotes nonradiative deactivation. For example, *fac*-tris(1-phenylpyrazolyl)iridium(III) (*fac*-Ir(ppz)$_3$) has strong blue phosphorescence (Φ_{PL} = 1.0) at 77 K, but has almost no emission at 298 K (Φ_{PL} = 0.001).[10,11] The last difficulty is the development of host and carrier transport materials. For blue phosphorescent materials, because of the high triplet excitation energy, confinement of the excitation energy is becoming difficult.[7]

Computational investigation of *fac*-Ir(ppy)$_3$ revealed that the HOMO is mainly localized at the iridium d-orbital and phenyl moiety, and the LUMO is localized at the pyridyl moiety. Therefore, control of the HOMO−LUMO energy gap has been attempted by the modification of green phosphorescent *fac*-Ir(ppy)$_3$ using the following three strategies. (1) One strategy is

Received: April 17, 2013

   dx.doi.org/10.1021/ic400950u | *Inorg. Chem.* XXXX, XXX, XXX−XXX

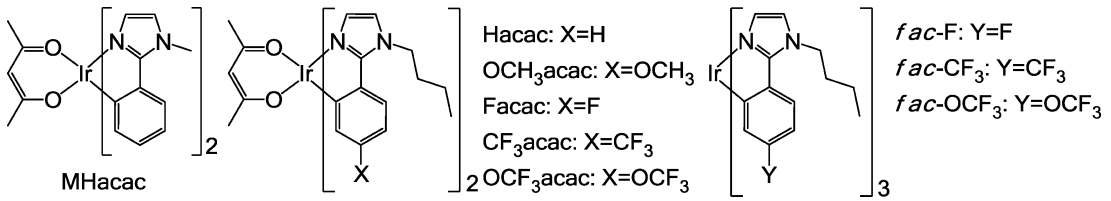

Figure 1. Complexes synthesized with phenylimidazole that have been studied.

stabilization of the HOMO by the introduction of electron withdrawing groups (EWGs) on a phenyl ring. Iridium(III) bis(4,6-difluorophenylpyridinato)acetylacetonate (FIr(acac)) and FIrpic exhibited very high efficiency emission;[7] λ_{max} for FIr(acac) is blue-shifted 40 nm compared with that for iridium(III) bis(2-phenylpyridinato)acetylacetonate (Ir(ppy)$_2$(acac)). These results indicate that the introduction of fluoro groups on the phenyl stabilizes the HOMO, because the HOMO is partly localized at the phenyl moiety. λ_{max} for *fac*-iridium(III) tris(4,6-difluorophenylpyridinate) (*fac*-Ir(dfppy)$_3$)[10] was the same as FIrpic (λ_{max} = 468 nm). De Cola and co-workers reported 3,4,6-trifluorophenyl derivative (*fac*-Ir(F$_3$ppy)$_3$) (459 nm), and 3,4,5,6-tetrafluorophenyl derivative (*fac*-Ir(F$_4$ppy)$_3$) (468 nm).[12] Interestingly, the increased number of F substitution, from three to four, resulted in red-shift of λ_{max}. These attempts demonstrate the effectiveness and limitations of design for blue phosphorescent Ir complexes by using EWGs. In addition, a device composed of FIrpic produced a large amount of defluorinated product,[13] bringing a shift to fluorine-free materials.[14](2) A second strategy is the use of strong EWG ancillary ligands: At the first stage, use of homoleptic complex was major. A typical preparation is conducted through a μ-Cl dimer complex; therefore, use of a diketonate complex through a dimer complex became more popular lately.[15] They are easily synthesized even they have equivalent or slightly lower emission efficiency than the homoleptic complexes.[16] Many types of ancillary ligands have been added to the complexes after FIrpic exhibited 20 nm (860 cm^{-1}) shorter λ_{max} than bis(4,6-difluorophenylpyridinato)acetylacetonate (FIracac). Changing the ancillary ligand to the EWG picolinate stabilized the HOMO. Thompson and co-workers reported iridium(III) bis(4,6-difluorophenylpyridinato)tetrakis(1-pyrazolyl)borate (FIr6) with borate as an ancillary ligand, and this complex had λ_{max} at 457 nm.[8] De Cola and co-workers reported that λ_{max} and Φ_{PL} of iridium(III) bis(4,6-difluorophenylpyridinato)-pyridyltriazole (FIrpyptz) were 461 nm and 0.27, respectively.[17] At this stage, pyridyl-azole type ligands became popular.[9,18] Chi and co-workers reported a phosphine type ligand;[19] iridium(III) bis(4,6-difluorophenylpyridinato)(2,4-difluorobenzyl)-diphenylphosphinate (FIrdfphdpp) had λ_{max} at 457 nm (Φ_{PL} = 0.19).[20] (3) The third strategy is breakaway from phenyl pyridinato complexes, using phenylheterocycles: Complexes with many types of ancillary ligands have been synthesized; however, the shift of λ_{max} was only 10 nm (392 cm^{-1}), and color clarity of the blue was less than satisfactory. Further blue-shift is very difficult using difluorophenylpyridine as a ligand; therefore, an approach to tune the resonance stabilization energy by changing the pyridyl group to other heterocycles was attempted. Complexes with phenyl pyrazole type ligand were reported.[10] *fac*-Ir(ppz)$_3$ and the 4,6-difluorophenyl derivatives *fac*-Ir(46dfppz)$_3$ exhibited phosphorescence at 77 K with λ_{max} at 414 and 390 nm, respectively. This was a significant blue-shift compared to phenyl pyridine based complexes such as *fac*-Ir(dfppy)$_3$ (λ_{max} = 450 nm). However, these complexes in solution were poorly phosphorescent at room temperature (Φ_{PL} < 0.001). Thompson and co-workers proposed that this was due to the bond weakness between iridium and the ligand nitrogen atoms, and they therefore synthesized a complex with a carbene type ligand, tris(1-phenyl-3-methylbenzimidazolin-2-ylidene)iridium(III) (Ir(pmb)$_3$).[11] However, its device external quantum efficiency was only 2.6%.[21] We examined the substituent effect of the Ir(pmb)$_3$. *fac*-Ir(CF$_3$pmb)$_3$ and *fac*-Ir(CH$_3$Opmb)$_3$ exhibited deep blue phosphorescence with λ_{max} at 396 and 403 nm (Φ_{PL} = 0.84 and 0.76), respectively.[22] However, there are no appropriate host and charge carrier materials for such large band gap complexes; therefore, the external quantum efficiency of the OLED device was only 2.6%.[21]

Samuel and co-workers reported a series of phenyl triazole type complexes.[23] The *fac*-iridium(III) tris(1-methyl-5-phenyl-3-propyl-[1,2,4]triazolate) (Ir(pptz)$_3$, *x*, *y* = 0.16, 0.20) and 4-fluorophenyl and 4,6-difluorophenyl derivatives (Ir(fpptz)$_3$ and Ir(dfpptz)$_3$, respectively) had λ_{max} at 449 nm (Φ_{PL} = 0.66), 428 (Φ_{PL} = 0.27), and 425 nm (Φ_{PL} = 0.03), respectively. Φ_{PL} decreased by the increase of the number of substituted fluorine atoms and increase of band gap energies.

There have been only a few reports of phenylimidazole derivatives. Grätzel and co-workers reported a diketonate complex, iridium(III) bis(1-methyl-2-phenylimidazolato)-acetylacetonate (N966),[24] which gives a broad emission between 440 and 800 nm that is applicable to a single molecular white lighting OLED. They also reported substituents effects for N966,[25] to improve efficiency up to Φ_{PL} = 0.95. Perumal and co-workers also reported substituent and solvent effects on the emission of diketonate complexes.[26] The aim of that research was to achieve white phosphorescence, and they did not deal with the blue phosphor. In addition, there is no report of homoleptic complexes.

In this study, we initiated blue phosphorescence-oriented research of phenylimidazolinato complexes. In particular, we have synthesized complexes with various substituents introduced on the phenyl ring (Figure 1), and examined their effects on the photophysical properties and frontier orbitals (HOMO and LUMO).

2. EXPERIMENTAL SECTION

2.1. General Information and Materials. All chemicals used for synthesis were purchased from Aldrich, Kanto Chemical, TCI, Wako Pure Chemical Industries, and Furuya Metal and used without further purification. Electroluminescence (EL) grade FIrpic was purchased from Luminescence Technology Corp. ^{1}H nuclear magnetic resonance (NMR) and ^{13}C NMR spectra were recorded on Jeol JNM-LA 400 and Bruker DPX 300 spectrometers. Fast atom bombardment and electrospray ionization (ESI) mass spectra were recorded on a Jeol JMS-AX500 double focusing mass spectrometer and Thermo Scientific Exactive mass spectrometer, respectively. Elemental analysis was conducted using an Exeter Analytical Inc. CE-440F analyzer.

dx.doi.org/10.1021/ic400950u | *Inorg. Chem.* XXXX, XXX, XXX−XXX

2.2. Synthesis of Ligands. Methyl-2-phenyl-1*H*-imidazole (MHpiH) was synthesized using the method reported.[27] The reaction yield was 38%, and details were described in the Supporting Information.

1-Butyl-2-(4-fluorophenyl)-1*H*-imidazole (FpiH) was synthesized using the method reported.[28] The reaction yield was 11%. Other ligands, 1-butyl-2-(4-(trifluoromethyl)phenyl)-1*H*-imidazole (CF_3piH), 1-butyl-2-(4-(trifluoromethoxy)phenyl)-1*H*-imidazole (OCF_3piH), 1-butyl-2-(4-methoxyphenyl)-1*H*-imidazole (OCH_3piH), and 1-butyl-2-phenyl-1*H*-imidazole (HpiH), were also synthesized using the same method, and their yields were 35%, 18%, 30%, and 36%, respectively, and details were described in the Supporting Information.

2.3. Synthesis of Homoleptic Complexes. The *fac*-tris[2-(4-trifluoromethylphenyl)-3-butyl-[1,3]-imidazolynato-C^2,N^1]iridium(III) complex (*fac*-CF_3) is given as an example.[29]

Iridium(III) trisacetylacetonate (763 mg, 1.56 mmol), CF_3piH (2.10 g, 7.83 mmol), and 9 mL glycerol that was deoxygenated by argon bubbling at 70 °C for 10 min were placed in a 50 mL three-necked flask. The mixture was stirred and heated up to 230 °C under nitrogen for 3.5 h. CH_2Cl_2 (60 mL) was added after cooling down to ambient temperature. An insoluble yellow precipitate was observed in the organic layer. AcOEt (40 mL) was added, and the precipitates were separated by filtration. The organic layer was washed twice with a mixture of water (100 mL) and sat. aq NaCl (40 mL), and then once with water, dried with anhydrous sodium sulfate, followed by solvent evaporation. The yellow powder was reprecipitated twice using CH_2Cl_2 and methanol to yield 398 mg. High-performance liquid chromatography (HPLC) analysis revealed that the reaction mixture contained equal amounts of the meridional isomer. Therefore, the powder was well stirred in 100 mL of CH_2Cl_2, and the residual facial isomer was obtained as ocher powder by filtration and dried under vacuum (156 mg, 0.16 mol, yield 10%). An HPLC chromatograph gave a single peak assigned to the facial isomer.

^{1}H NMR (CD_2Cl_2, 300 MHz, 300 K): δ (ppm) 7.47 (d, J = 8.2 Hz, 3H), 7.10 (d, J = 8.2 Hz, 3H), 7.06 (s, 3H), 6.90 (d, J = 1.4 Hz, 3H), 6.37 (d, J = 1.4 Hz, 3H), 4.44−4.23 (m, 6H), 1.93−1.83 (m, 6H), 1.48−1.36 (m, 6H), 0.96 (t, J = 7.4 Hz, 9H).

ESI-MS: m/z = 995.3013, theoretical mass = 995.3029, δ = −1.60 ppm.

Anal. Calcd for $C_{42}H_{42}F_9IrN_6$: C, 50.75; H, 4.26; N, 8.45. Found: C, 50.63; H, 4.26; N, 8.29.

The *fac*-tris[2-(4-trifluoromethoxyphenyl)-3-butyl-[1,3]-imidazolynato-C^2,N^1]iridium(III) complex (*fac*-OCF_3) was obtained as an ocher powder (yield 23%) using the same method.

^{1}H NMR (CD_2Cl_2, 300 MHz, 300 K): δ (ppm) 7.40 (d, J = 8.5 Hz, 3H), 6.86 (d, J = 1.4 Hz, 3H), 6.72 (d, J = 8.5 Hz, 3H), 6.67 (s, 3H), 6.35 (d, J = 1.4 Hz, 3H), 4.37−4.19 (m, 6H), 1.93−1.80 (m, 6H), 1.49−1.37 (m, 6H), 0.97 (t, J = 7.3 Hz, 9H).

ESI-MS: m/z = 1043.2870, theoretical mass = 1043.2877, δ = −0.65 ppm.

Anal. Calcd for $C_{42}H_{42}F_9IrN_6O_3$: C, 48.41; H, 4.06; N, 8.07. Found: C, 48.23; H, 3.96; N, 7.82.

The *fac*-tris[2-(4-fluorophenyl)-3-butyl-[1,3]imidazolynato-C^2,N^1]-iridium(III) complex (*fac*-F) was obtained as an ocher powder (yield 1%) using the same method.

^{1}H NMR (CD_2Cl_2, 300 MHz, 300 K): δ (ppm) 7.36 (dd, J = 8.2 Hz, J_{FH} = 5.6 Hz, 3H), 6.82 (d, J = 1.3 Hz, 3H), 6.60−6.51 (m, 6H), 6.30 (d, J = 1.3 Hz, 3H), 4.37−4.17 (m, 6H), 1.93−1.82 (m, 6H), 1.49−1.37 (m, 6H), 0.97 (t, J = 7.3 Hz, 9H).

ESI-MS: m/z = 845.3115, theoretical mass = 845.3125, δ = −1.17 ppm.

Anal. Calcd for $C_{39}H_{42}F_3IrN_6$: C, 55.50; H, 5.02; N, 9.96. Found: C, 55.21; H, 4.95; N, 9.71.

2.4. Syntheses[15,30] of Diketonate Complexes. Iridium(III) bis[2-(4-fluorophenyl)-3-butyl-[1,3]-imidazolynato-C^2,N^1]-acetylacetonate (Facac) is given as an example.

A mixture of iridium(III) chloride *n*-hydrate (201 mg, 0.54 mmol), FpiH (293 mg, 1.34 mmol), 2-ethoxyethanol (30 mL), and H_2O (10 mL) were set in the flask, purged with nitrogen, and stirred for 6 h at 110 °C. After cooling to ambient temperature, water (100 mL) and brine (30 mL) were added. The organic layer was extracted three times with CH_2Cl_2. The solvent was removed *in vacuo*, and crude μ-Cl dimer complex was obtained. A mixture of acetylacetone (250 mg, 2.50 mmol) and potassium carbonate (354 mg, 2.56 mmol) in 25 mL of 2-ethoxyethanol was added, and this reaction mixture was stirred for 6 h at 110 °C. After cooling to ambient temperature, water (100 mL) and brine (30 mL) were added. The organic layer was extracted three times with CH_2Cl_2. Brown powder was obtained after removal of the solvent *in vacuo*. The product was purified by precipitation (CH_2Cl_2 and hexane) after the column chromatography (alumina, CH_2Cl_2), and the complex was obtained as a pale yellow powder (52 mg, 13%).

^{1}H NMR ($CDCl_3$, 300 MHz, 300 K): δ (ppm) 7.28−7.26 (m, 2H), 6.99 (d, J = 1.4 Hz, 2H), 6.92 (d, J = 1.4 Hz, 2H), 6.74−6.69 (m, 2H), 6.62−6.57 (m, 2H), 6.37−6.35 (m, 2H), 5.15 (s, 1H), 4.46−4.27 (m, 4H), 2.00−1.90 (m, 4H), 1.77 (s, 6H), 1.53−1.41 (m, 4H), 1.00 (t, J = 7.4 Hz, 6H).

ESIMS: m/z = 749.2236, theoretical mass = 749.2250, δ = −1.85 ppm.

Anal. Calcd for $C_{31}H_{35}F_2IrN_4O_2$: C, 51.30; H, 4.86; N, 7.72. Found: C, 51.42; H, 4.78; N, 7.48.

The iridium(III) bis[2-(4-trifluoromethylphenyl)-3-butyl-[1,3]-imidazolynato-C^2,N^1]acetylacetonate (CF_3acac) was obtained as yellow powder (yield 63%) using the same method.

^{1}H NMR ($CDCl_3$, 300 MHz, 300 K): δ (ppm) 7.32 (d, J = 7.5 Hz, 2H), 7.04 (d, J = 1.5 Hz, 2H), 7.02 (d, J = 1.5 Hz, 2H), 6.97 (d, J = 7.5 Hz, 2H), 6.46 (s, 2H), 5.19 (s, 1H), 4.58−4.22 (m, 4H), 1.95−1.87 (m, 4H), 1.80 (s, 6H), 1.51−1.39 (m, 4H), 0.98 (t, J = 7.3 Hz, 6H).

ESIMS: m/z = 827.2347, theoretical mass = 827.2366, δ = −2.35 ppm.

Anal. Calcd for $C_{33}H_{35}F_6IrN_4O_2$: C, 47.99; H, 4.27; N, 6.78. Found: C, 48.18; H, 4.15; N, 6.91.

The iridium(III) bis[2-(4-trifluoromethoxyphenyl)-3-butyl-[1,3]-imidazolynato-C^2,N^1]acetylacetonate (OCF_3acac) was obtained as yellow powder (yield 41%) using the same method.

^{1}H NMR (CD_2Cl_2, 300 MHz, 300 K): δ (ppm) 7.33 (d, J = 8.5 Hz, 2H), 7.06 (d, J = 1.5 Hz, 2H), 6.97 (d, J = 1.5 Hz, 2H), 6.68 (dd, J = 8.5 and 1.3 Hz, 2H), 6.07 (d, J = 1.3 Hz, 2H), 5.22 (s, 1H), 4.49−4.26 (m, 4H), 1.98−1.88 (m, 4H), 1.79 (s, 6H), 1.51−1.41 (m, 4H), 0.99 (t, J = 7.4 Hz, 6H).

ESIMS: m/z = 859.2247, theoretical mass = 859.2265, δ = −2.07 ppm.

Anal. Calcd for $C_{33}H_{35}F_6IrN_4O_4$: C, 46.20; H, 4.11; N, 6.53. Found: C, 46.17; H, 4.11; N, 6.52.

The iridium(III) bis[2-(4-methoxyphenyl)-3-butyl-[1,3]-imidazolynato-C^2,N^1]acetylacetonate (OCH_3acac) was obtained as pale yellow powder (yield 20%) using the same method.

^{1}H NMR ($CDCl_3$, 300 MHz, 300 K): δ (ppm) 7.20 (d, J = 8.5 Hz, 2H), 6.94 (d, J = 1.4 Hz, 2H), 6.84 (d, J = 1.4 Hz, 2H), 6.30 (dd, J = 8.5 and 2.6 Hz, 2H), 5.90 (d, J = 2.6 Hz, 2H), 5.14 (s, 1H), 4.40−4.18 (m, 4H), 3.55 (s, 6H), 1.96−1.86 (m, 4H), 1.77 (s, 6H), 1.52−1.39 (m, 4H), 0.98 (t, J = 7.4 Hz, 6H).

ESIMS: m/z = 750.2732, theoretical mass = 750.2752, δ = −2.54 ppm.

Anal. Calcd for $C_{33}H_{41}IrN_4O_4$: C, 52.85; H, 5.51; N, 7.47. Found: C, 52.51; H, 5.45; N, 7.34.

The iridium(III) bis[2-phenyl-3-butyl-[1,3]-imidazolynato-C^2,N^1]-acetylacetonate (Hacac) was obtained as yellow powder (yield 18%) using the same method.

^{1}H NMR ($CDCl_3$, 300 MHz, 300 K): δ (ppm) 7.27 (d, J = 7.5 Hz, 2H), 6.99 (d, J = 1.4 Hz, 1H), 6.92 (d, J = 1.4 Hz, 1H), 6.72 (dt, J = 7.5 and 1.2 Hz, 2H), 6.60 (dt, J = 7.5 and 1.3 Hz, 2H), 6.36 (dd, J = 7.5 and 1.2 Hz, 2H), 5.15 (s, 1H), 4.46−4.27 (m, 4H), 2.00−1.90 (m, 4H), 1.77 (s, 6H), 1.53−1.41 (m, 4H), 1.00 (t, J = 7.4 Hz, 6H).

ESIMS: m/z = 690.2511, theoretical mass = 690.2540, δ = −4.24 ppm.

Anal. Calcd for $C_{31}H_{37}IrN_4O_2$: C, 53.97; H, 5.41; N, 8.12. Found: C, 53.72; H, 5.37; N, 7.85.

dx.doi.org/10.1021/ic400950u | *Inorg. Chem.* XXXX, XXX, XXX−XXX

Iridium(III) bis[2-phenyl-3-methyl-[1,3]-imidazolynato-C^2,N^1]-acetylacetonate (MHacac) was obtained as yellow powder (yield 47%) using the same method.

^{1}H NMR ($CDCl_3$, 300 MHz, 300 K): δ (ppm) 7.36 (d, J = 7.5 Hz, 2H), 6.99 (d, J = 1.4 Hz, 2H), 6.89 (d, J = 1.4 Hz, 2H), 6.73 (t, J = 7.5 Hz, 2H), 6.63 (t, J = 7.5 Hz, 2H), 6.40 (d, J = 7.5 Hz, 2H), 5.15 (s, 1H), 4.10 (s, 6H), 1.78 (s, 6H).

ESIMS: m/z = 629.1475, theoretical mass = 629.1499, δ = −3.87 ppm.

Anal. Calcd for $C_{25}H_{25}IrN_4O_2$: C, 49.57; H, 4.16; N, 9.25. Found: C, 49.31; H, 4.05; N, 8.99.

2.5. X-ray Crystallography. Single crystals of *fac*-CF_3 and *fac*-OCF_3 were grown in CH_2Cl_2−hexane. Diffraction data were collected on Bruker SMART APEX II CCD diffractometer at 173 K with graphite-monochromated Mo Kα radiation. Initial atomic positions were determined using direct methods. The structures of the compound were refined using least-squares methods with the XShell program. ORTEP[31] and packing diagrams were constructed using Mercury 3.0.[32] Optical micrographs of the single crystals were obtained with a microscope (Olympus DP71).

2.6. Electrochemistry. Cyclic voltammetry (CV) was performed using a standard compartment cell equipped with a Pt working electrode (BAS), a platinum wire counter electrode, a Ag/Ag^+ ($Ag/AgNO_3$) reference electrode, and a ALS/CH Instruments model 440A analyzer. Argon-purged anhydrous tetrahydrofuran (THF) was used as a solvent, and tetrabutylammonium hexafluorophosphate (0.1 M) was used as a supporting electrolyte. The scan rate was 100 mV/s. The HOMO energy level was estimated using the value of ferricenium/ferrocene couple (4.8 eV[33]) and a potential increase of 100 mV by using eq 1.

$$E_{HOMO} = (E_{HOMO}^{ferrocene} - E_{onset}^{ferrocene}) + E_{onset} = 4.8 - 0.1 + E_{onset} \quad (1)$$

2.7. Photophysical Properties. UV−vis absorption spectra were measured using a Jasco V570 spectrophotometer. Photoluminescence (PL) spectra were measured using a Jasco F6010 fluorescence spectrophotometer. PL lifetimes were measured using a Horiba NAES-550 single photon counting spectrophotometer. Stabilizer-free anhydrous 2-MeTHF (refluxed and distilled over sodium metal) was used as a solvent for PL quantum yield and PL lifetime measurements. A rectangular quartz cuvette equipped Pyrex tube was placed attaching to a metal block in the spectrometer and maintained at a temperature constant. The Pyrex tubes were submerged into a liquid-nitrogen-filled Dewar flask equipped with a rectangular quartz optical window (77 K). Sample solutions in 2-MeTHF were carefully deaerated using three freeze−pump−thaw cycles. Emission quantum yields were determined at 298 K using quinine sulfate dehydrate as a standard (in 0.5 M sulfuric acid, excitation at 365 nm, Φ_{PL} = 0.546[34,35]). *fac*-Ir(ppz)$_3$ was used as a standard (Φ_{PL} = 1.0 in 2-MeTHF) at 77 K.[36] The refractive index of 2-MeTHF at 298 K was 1.405 08.[37] Chromaticity coordinates were measured using a Konica Minolta CS-100A luminance meter. The radiative (k_r) and nonradiative (k_{nr}) rate constants were calculated from Φ_{PL} and τ using the following equations (eqs 2 and 3):

$$\Phi_{PL} = k_r/(k_r + k_{nr}) \quad (2)$$

$$\tau = 1/(k_r + k_{nr}) \quad (3)$$

2.8. DFT and Time Dependent (TD)-DFT Calculations. DFT and TD-DFT calculations were performed using the Gaussian 03 package[38] at the RB3LYP[39]/ LANL2DZ[40] level. The structures were fully optimized, and TD-DFT calculations were performed with the ground-state geometry to obtain the vertical excitation energies of the low-lying singlet and triplet excited state of the complexes. The contributions to the HOMO and LUMO were calculated using Gauss Sum (ver 2.2).[41]

2.9. Fabrication of OLED Devices. The EL devices were fabricated with the following configuration: Indium tin oxide (ITO)/poly(styrenesulfonate)-doped poly(3,4-ethylenedioxythiophene) (PEDOT:PSS, 40 nm)/light emitting layer (50 nm)/bathocuproine (BCP) (20 nm)/CsF (2 nm)/Al (100 nm). PEDOT was spin-coated directly onto the ITO glass and dried at 200 °C for 10 min. 3,3″,5,5″-Tetra(9*H*-carbazol-9-yl)-1,1′:3′,1″-terphenyl (mB-4Cz)[42] was synthesized and used as a wet processable host material. The light emitting layer was spin-coated on the PEDOT layer using 1,2-dichloroethane as a solvent, and dried at 60 °C for 3 h under vacuum. The BCP layer, which was grown by thermal sublimation in a vacuum of 2 × 10^{-6} Torr, was used as an electron transport layer that blocked holes and confined excitons. The cathode CsF/Al alloy was subsequently deposited onto the BCP layer using an Ulvac VPC 1100 vacuum deposition system.

3. RESULTS AND DISCUSSION

3.1. Synthesis and Molecular Structure. We have synthesized nine homo- and heteroleptic iridium complexes, as detailed in the Experimental Section. 1-Methyl-2-phenyl-1*H*-imidazole (MHpiH) was obtained by methylation of 2-phenylimidazole using dimethyl carbonate.[27] However, other ligands have *n*-butyl chains on the imidazolyl ring and substituents on the phenyl ring; therefore, a one-pot synthesis method has been applied to easily obtain reactants and save time.[28] Introduction of the *n*-butyl group helps to increase the stability[43] and solubility of the complexes. All ligand were obtained as liquids and yields were 38% (MHpiH) and between 11% and 36% (one-pot syntheses).

Diketonate iridium(III) complexes were synthesized through the μ-Cl dimer complexes obtained from iridium(III) trischloride *n*-hydrate and corresponding ligand molecules.[15,30] Purification by silica gel chromatography gave a brownish eluent solution, which indicates some decomposition; however, the product was successfully purified using alumina chromatography. The yields were 63% for CF_3acac, around 40% for OCF_3acac and MHacac, and 10−20% for others.

At first, it was considered that the homoleptic complexes could be synthesized through the diketonate complexes;[15] however, the cyclometalated ligand exchange reaction of iridium(III) trisacetylacetonate was employed to save time.[28] We have successfully synthesized CF_3piH (10%), OCF_3piH (23%), and FpiH (1%) with relatively low yields (yields in parentheses).

Single crystals of homoleptic complexes of *fac*-CF_3 and *fac*-OCF_3 were grown using a method with *n*-hexane vapor diffused into CH_2Cl_2. The resultant crystals were brown and had a distorted hexagonal columnar shape (Figure S1, Supporting Information). X-ray crystallographic data including essential bond lengths are listed in Table 1 and Table S1 in the Supporting Information.

ORTEP diagrams[31] of *fac*-CF_3 and *fac*-OCF_3 are presented in Figure 2. Three cyclometalated ligands were hexagonally coordinated around the iridium metal center. There was little variation in the lengths of each of the three Ir−N and Ir−C

Table 1. Bond Lengths for *fac*-CF_3, *fac*-OCF_3, and *fac*-Ir(tfmppz)$_3$

	bond distance [Å]		
bond type	*fac*-CF_3	*fac*-OCF_3	*fac*-Ir(tfmppz)$_3$[10]
Ir1−C1	2.018(3)	2.019(2)	2.016(8)
Ir1−C2	2.017(4)	2.019(2)	2.016(8)
Ir1−C3	2.018(3)	2.018(3)	2.013(8)
Ir1−N1	2.109(3)	2.105(2)	2.114(7)
Ir1−N2	2.108(4)	2.105(2)	2.113(7)
Ir1−N3	2.108(3)	2.106(3)	2.116(8)

dx.doi.org/10.1021/ic400950u | Inorg. Chem. XXXX, XXX, XXX−XXX

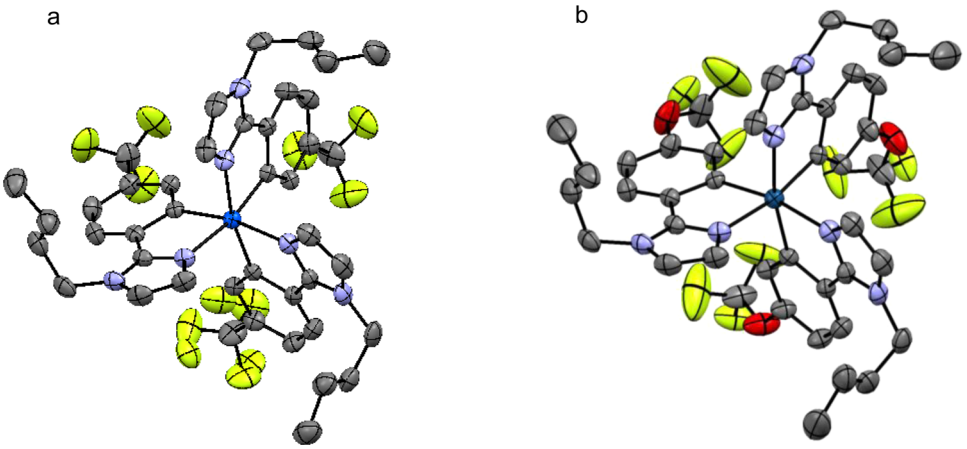

Figure 2. ORTEP diagram of (a) *fac*-CF_3 and (b) *fac*-OCF_3 (hydrogen atoms are neglected for clarity).

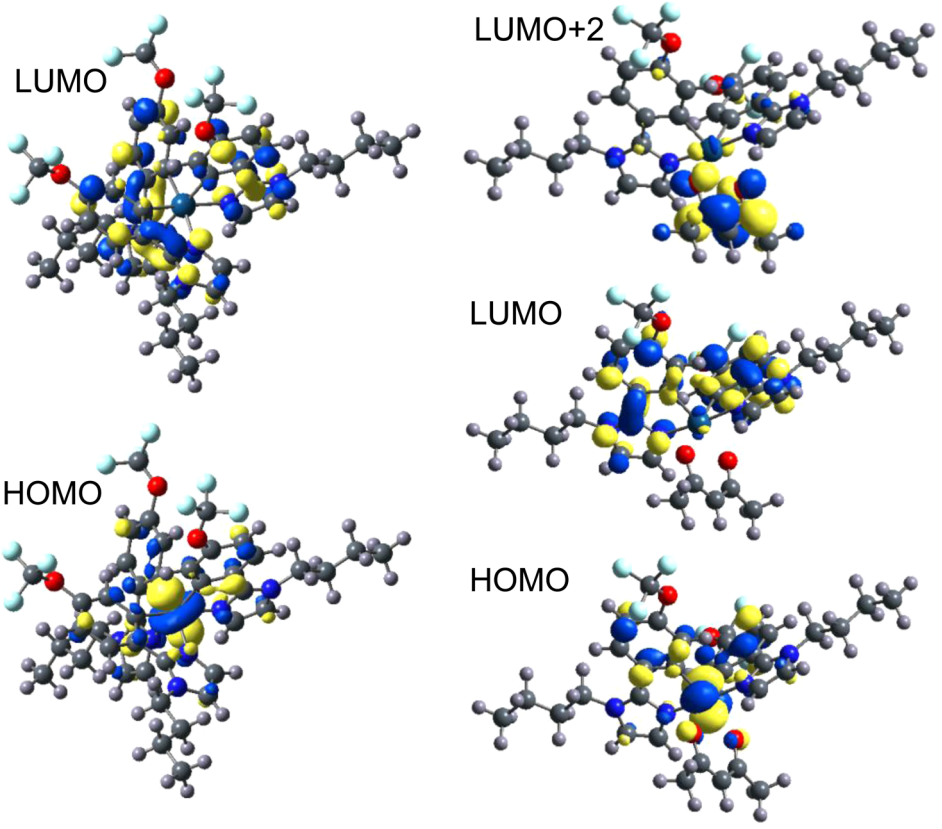

Figure 3. MOs of *fac*-OCF_3 (left side) and OCF_3acac (right side).

bonds, which indicates high symmetry. Disorder was observed for the trifluoromethoxy group of *fac*-OCF_3. A similar complex with trifluoromethyl substituents, *fac*-tris(1-(4-(trifluoromethyl)phenyl)pyrazolato) iridium(III) (*fac*-Ir-(tfmppz)$_3$), was reported by Thompson, which had similar bond lengths.[10] The packing diagram indicates that the rhombohedral lattice is composed of a pair of optical isomers; i.e., these are racemic crystals (Figure S2 in Supporting Information). A combination of three rhombohedral lattices results in hexagonal columnar crystals.

In contrast, the CF_3acac and OCF_3acac diketonate complexes gave fine needle-like crystals. Therefore, we have not succeeded in measuring single crystal X-ray diffraction. MHacac (N966 in ref 25) has been reported to have a meridional configuration; therefore, other diketonate complexes may also have similar structures.

3.2. DFT Calculation. Complex structures were optimized using the DFT method with the B3LYP/LANL2DZ basis set level.[23,44] Optimized structures and the HOMO−LUMO of *fac*-OCF_3 and OCF_3acac are plotted in Figure 3. For the molecular orbitals (MOs), the atomic orbital coefficients of each component, such as iridium metal (Ir), phenyl (Ph), imidazolyl (Im), pyridyl (Py), and acetylacetone (acac) moieties, are obtained using the Gauss Sum program, as shown in Table 2.

The Ir−C (mean value 2.042 Å) and Ir−N (mean value 2.127 Å) bond lengths in *fac*-OCF_3 were obtained by structural optimization and are similar to the Ir−C (mean value 2.019 Å)

dx.doi.org/10.1021/ic400950u | *Inorg. Chem.* XXXX, XXX, XXX−XXX

Table 2. Calculated Energy Levels of the HOMO, LUMO, LUMO + 1, and LUMO + 2 and Contribution of Iridium Metal (Ir), Phenyl (Ph), Imidazolyl (Im), Pyridyl (Py), and Acetylacetonate (acac) Moieties

		Ir	Ph	Im or Py	acac	E [eV]
fac-CF_3	LUMO	0.4	64.1	35.5		1.49
	HOMO	56.0	30.7	13.3		5.11
fac-OCF_3	LUMO	0.5	57.0	42.5		1.19
	HOMO	53.2	31.8	15.0		5.11
fac-F	LUMO	0.6	53.6	45.8		0.77
	HOMO	52.4	32.8	14.8		4.73
CF_3acac	LUMO + 2	2.2	1.2	1.0	95.6	1.05
	LUMO + 1	2.8	60.3	34.3	2.6	1.41
	LUMO	1.6	62.3	35.7	0.4	1.54
	HOMO	48.8	36.8	8.6	5.8	5.16
OCF_3acac	LUMO + 2	2.8	10.5	8.8	77.9	1.03
	LUMO + 1	2.2	43.0	34.5	20.3	1.15
	LUMO	1.9	55.4	42.3	0.4	1.25
	HOMO	47.6	37.0	9.9	5.5	5.16
Facac	LUMO + 2	3.6	42.3	39.7	14.4	0.74
	LUMO + 1	1.4	7.5	7.4	83.7	0.87
	LUMO	2.1	51.9	45.6	0.4	0.88
	HOMO	46.4	38.4	10.2	5.0	4.86
OCH_3acac	LUMO + 2	3.0	46.4	46.2	4.4	0.31
	LUMO + 1	2.0	50.9	46.8	0.3	0.43
	LUMO	1.6	2.2	2.6	93.6	0.54
	HOMO	46.4	38.9	10.0	4.6	4.43
Hacac	LUMO + 2	3.6	42.2	39.8	14.4	0.50
	LUMO + 1	2.1	51.7	45.8	0.4	0.64
	LUMO	1.4	7.4	7.4	83.8	0.64
	HOMO	47.0	39.8	8.4	4.8	4.48
MHacac	LUMO + 2	3.7	37.6	36.4	22.3	0.59
	LUMO + 1	1.4	11.4	11.3	75.9	0.71
	LUMO	2.1	51.2	46.3	0.4	0.73
	HOMO	47.1	39.8	8.2	4.9	4.56
fac-$Ir(ppy)_3$[9]	LUMO	0.2	25.9	73.5		1.47
	HOMO	52.8	38.9	8.2		4.95

and Ir−N (mean value 2.105 Å) bond lengths obtained by X-ray crystallography. The Ir−C (mean value 2.017 Å) and Ir−N (mean value 2.042 Å) bond lengths obtained by DFT for OCF_3acac are shorter than those of *fac*-OCF_3. The results correspond to the X-ray crystallographic results for *fac*-tris(2-(*p*-tolyl)pyridinato) iridium(III) (*fac*-$Ir(tpy)_3$) and iridium(III) bis(2-(*p*-tolyl)pyridinato)- acetylacetonate ($Ir(tpy)_2$(acac)) reported by Thompson.[11]

MO analysis indicated that the HOMO is mainly localized in the d-orbital (46.4−56.0%) and phenyl moiety (30.7−39.8%). Similar behavior has been observed in *fac*-$Ir(ppy)_3$[23] and *fac*-$Ir(ppz)_3$.[44] More detailed analysis of the MOs of *fac*-CF_3, *fac*-OCF_3, and *fac*-F revealed the HOMO contribution of the phenyl moiety was 30.7−32.8%, which is smaller than that of *fac*-$Ir(ppy)_3$ (38.9%). Accordingly, the contribution of the imidazole ring part (13.3−15.0%) is higher than that of the pyridine part (8.2%) in *fac*-$Ir(ppy)_3$. On the other hand, the contributions of phenyl ring and heterocyclic ring parts of diketonate complexes were similar to those of *fac*-$Ir(ppy)_3$; however, the contribution of the iridium d-orbital had smaller values 46−48%, and these decreases appeared with an increase of acetylacetone parts (4.6−5.8%). Therefore, in *fac*-CF_3, *fac*-OCF_3, and *fac*-F, the substitution of EWGs on the phenyl ring is less effective to stabilize the HOMO than in the case of *fac*-$Ir(ppy)_3$.

The LUMO localized on the ligand (nearly 100%) is the same result as that for *fac*-$Ir(ppy)_3$[23] and *fac*-$Ir(ppz)_3$.[44] These results strongly indicate a HOMO−LUMO transition with MLCT character. Details of the LUMO in the phenyl (Ph) moieties (53.6−64.1%) of homoleptic *fac*-CF_3, *fac*-OCF_3, and *fac*-F have a higher contribution than those of the imidazolyl (Im) parts (35.5−45.8%); therefore, these populations are quite different from the LUMO of *fac*-$Ir(ppy)_3$[23] with 73.5% pyridyl (Py) and 25.9% phenyl moieties. The LUMO of diketonate complexes also has a higher coefficient at the phenyl moiety (51.2−62.3%) than at the imidazole moiety (35.7−46.3%), similar to the homoleptic complexes. However, there are two exceptions, OCH_3acac and Hacac, where the LUMO is localized at acetylacetone (93.6% and 83.8%, respectively). In addition to these two extreme cases, other diketonate complexes have a LUMO + 1 (MHacac and Facac) or LUMO + 2 (CF_3acac and OCF_3acac) localized at acetylacetone (e.g., Figure 3, right side). Complexes with trifluoromethyl substituents, *fac*-CF_3 and CF_3acac, have LUMO highly localized at the phenyl moiety with 64.1% and 62.3%, respectively.

The calculated results indicate that the HOMOs of iridium phenylimidazolinate complexes have similar or slightly smaller contributions at the phenyl moiety, as with *fac*-$Ir(ppy)_3$; however, much larger localization of the LUMO at the phenyl moiety. Therefore, substitution of the phenyl group by EWGs affects not only the HOMO, but also the LUMO. This type of HOMO−LUMO relation has also been reported for iridium phenyltriazolinate complexes.[23]

3.3. Electrochemical Properties. Oxidation potentials were determined by cyclic voltammetry in anhydrous THF to estimate the effect of substituents on the HOMO energy level. Voltammograms are shown in Figure S3 in the Supporting Information, and the results are summarized in Table 3. All of the complexes showed poor reversibility for oxidation voltammograms. Complexes having F-atom, such as OCF3acac, Facac, fac-F, and complex Hacac, showed reversibilities that were not good. All the complexes examined gave irreversible reduction potentials. Samuel, Ma, and their co-workers reported difficulty in observing reversible reduction potentials for blue phosphorescent complexes.[23,44] These instabilities may reflect on the OLED device instability. Grätzel and co-workers reported the oxidation potential of MHacac (N966)[25] and estimated the HOMO energy level to be 4.97 eV. In the present experiment, the value is estimated to be 4.91 eV by the same method as that given in the literature. The results of DFT

Table 3. HOMO Energy Levels Corresponding to the Rise-Up Potentials of Oxidative Cyclic Voltammograms

	E_{onset} [mV]	E_{HOMO} [eV]
fac-CF_3	237	5.04
fac-OCF_3	210	5.00
fac-F	161	4.96
CF_3acac	222	5.02
OCF_3acac	377	5.18
Facac	307	5.11
OCH_3acac	92	4.89
Hacac	159	4.96
MHacac	118	4.92
ferrocene	100	4.8[33]

dx.doi.org/10.1021/ic400950u | Inorg. Chem. XXXX, XXX, XXX−XXX

calculations indicate that the HOMO of these complexes is localized at the d-orbital of iridium and the π-orbital of the phenyl moiety. The oxidation potentials shift toward the more oxidative direction by substitution with EWGs. This is explained by the stabilization of the HOMO due to delocalization of the iridium d-orbital electron toward the phenyl π-orbitals by substitution with EWGs. On the other hand, the substitution of electron donating groups (EDGs) induces destabilization of the HOMO, which is observed as a more negative shift of the oxidation peak potential.

The Swain−Lupton constant,[45] as a modification of the Hammett rule, is used as an electron accepting and donating parameter, as shown in Table 4. A larger F value is more σ-electron inductive (inductive effect), and a smaller R is more π-electron donative (resonance effect). While the F value of the F substituent has the highest value at 0.45, *fac*-F and Facac have oxidation potentials that are 50−70 mV smaller than those of *fac*-OCF_3 and OCF_3acac. This is explained by the small R value of −0.39 for the F atom due to the π-electron donating ability of the nonbonding lone-pair electrons, which results in destabilization of the HOMO.

Table 4. Substituents and their Swain−Lupton Constants[45]

	F value	R value
CF_3	0.38	0.16
OCF_3	0.39	−0.04
F	0.45	−0.39
OCH_3	0.29	−0.56
H	0.03	0.00
CH_3	0.01	−0.18
$(CH_2)_3CH_3$	−0.01	−0.15

The *fac*-CF_3 complex has an oxidation potential 15 mV smaller than that of CF_3acac, which is explained by the stronger electron donating ability of the phenylimidazole ligand compared with that of acetylacetone, and this causes destabilization of the iridium d-orbital.

For further investigation, the HOMO energy levels (E_{HOMO}) derived from the oxidation potentials are listed in Table S2 in the Supporting Information. Complexes substituted with trifluoromethyl groups, *fac*-Ir(tfmppz)$_3$, *fac*-Ir(tfmpmb)$_3$, and *fac*-Ir(tfmptz)$_3$, have E_{HOMO} values in the range 5.4−5.5 eV,[10,22,23] and the *fac*-CF_3 imidazolinato complex has E_{HOMO} = 5.04 eV. This value is smaller than that for *fac*-Ir(ppy)$_3$: E_{HOMO} = 5.11 eV.[10] This provides an important insight: that phenylimidazolinato complexes examined in this paper have higher HOMO energy levels, by approximately 0.4 eV, than those of complexes with similar skeleton structures, such as phenylpyridinato, phenylpyrazolato, phenylimidazolinato carbene type, and phenyltriazolato complexes. Thus, this nature is due to the imidazole moiety.[46]

3.4. Absorption Spectra. UV−vis absorption spectra of complexes measured in 2-MeTHF are shown in Figure 4. The absorption maxima (λ_{max}) and molar extinction coefficients (ε) are summarized in Table 5. Triplet excitation energies (E_g) were assumed using the following equation (eq 4), where λ_{onset} is the rise-up wavelengths of weak spin-forbidden ^{3}MLCT absorptions, h is the Planck constant, c is light speed, and e is electron charge.

$$E_g = hc/e\lambda_{onset}[\mathrm{eV}] \quad (4)$$

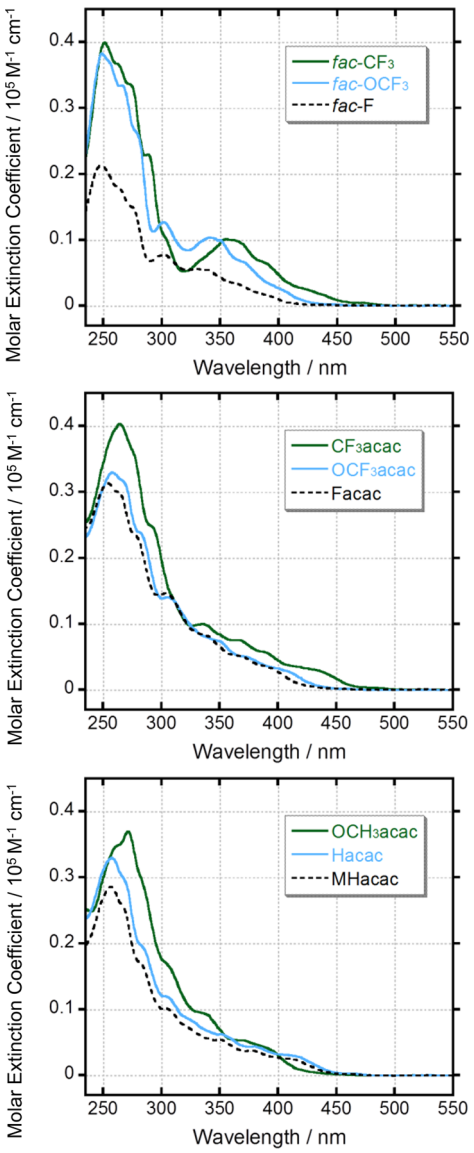

Figure 4. Absorption spectra in 2-MeTHF at 298 K.

Table 5. Characteristics of Absorption Spectra in 2-MeTHF Measured at 298 K[a]

	λ_{abs} (log ε) [nm]	λ_{onset} [nm]	E_g [eV]
fac-CF_3	251 (4.60), 273 (4.53, sh), 288 (4.36), 355 (4.01)	460	2.70
fac-OCF_3	249 (4.58), 266 (4.53, sh), 302 (4.11), 341 (4.02)	428	2.90
fac-F	248 (4.33), 302 (3.89), 331 (3.75)	413	3.00
CF_3acac	265 (4.61), 336 (4.01), 366 (3.88, sh)	466	2.66
OCF_3acac	258 (4.52), 304 (4.15, sh)	436	2.84
Facac	253 (4.50), 304 (4.17, sh)	423	2.93
OCH_3acac	271 (4.57), 370 (3.73, sh)	423	2.93
Hacac	257 (4.52), 303 (4.08, sh), 351 (3.80, sh), 379 (3.65, sh)	449	2.76
MHacac	256 (4.46), 303 (4.00, sh), 350 (3.73, sh)	445	2.79

[a]sh in parenthese indicates a peak observed as a shoulder.

The absorption band of iridium complexes can be generally separated into two regions. The absorption band below 290 nm is assigned to the spin-allowed ^{1}LC (ligand-centered) transition

dx.doi.org/10.1021/ic400950u | Inorg. Chem. XXXX, XXX, XXX−XXX

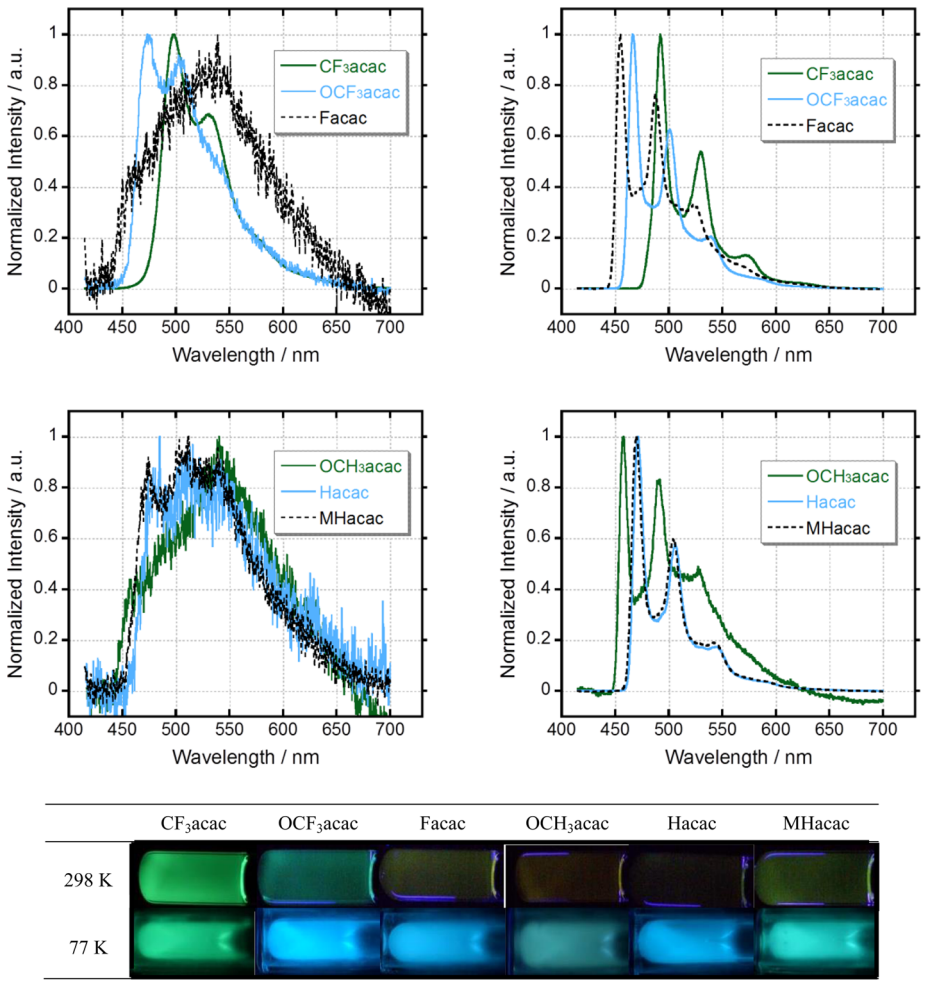

Figure 5. Phosphorescence spectra of diketonate complexes measured in 2-MeTHF (at 298 K, left side) and in a glassy matrix (at 77 K, right side). Photographs of phosphorescence of diketonate complexes measured in 2-MeTHF (at 298 K) and in a glassy matrix (at 77 K).

of the phenylimidazole moiety. The band around 350 nm is assigned to spin-allowed ^{1}MLCT. Bands longer than ^{1}MLCT are assigned to a mixture of spin-forbidden ^{3}LC and ^{3}MLCT. For the homoleptic complexes, the ^{1}MLCT absorption band appeared as a moderate peak; however, the diketonate complexes showed a gradual decrease of absorption, as similarly reported for *fac*-Ir(ppz)$_3$ and Ir(ppz)$_2$(acac).[44] The change of E_g by the introduction of substituents will be discussed in section 3.5.

3.5. Phosphorescence Spectra, Quantum Yields, and Lifetimes. Phosphorescence spectra of the complexes measured in deaerated 2-MeTHF are shown in Figure 5. The characteristic phosphorescence data, such as emission λ_{max} and chromaticity coordinates, are summarized in Table 6. In addition, the quantum yield (Φ_{PL}) at 298 and 77 K, and lifetimes (τ) at 298 K measured using the single-photon counting method, are listed in Table 7. Emission decay profiles for the homoleptic and CF$_3$acac complexes showed single exponential characteristics. Diketonate complexes other than CF$_3$acac showed double-exponential decay. One component has a decay time of a microsecond, and another has less than a couple of nanoseconds. The lifetime of MHacac in CH_2Cl_2 was reported to be 24 ns.[25]

In the case of the diketonate complexes at 298 K, only the CF$_3$acac complex showed strong phosphorescence (Φ_{PL} = 0.28), whereas the other complexes showed broad emission within 450−700 nm with poor Φ_{PL} < 0.01. Φ_{PL} for MHacac was 0.0026, which is smaller than that reported for N966 (Φ_{PL} = 0.015[25]). This may be caused by solvent polarity; the

Table 6. Phosphorescence Characteristics

	λ_{max} [nm]		CIE coordinates (x, y)	
	298 K	77 K	298 K	77 K
fac-CF$_3$	486, 518	483, 520, 560	(0.246, 0.467)	(0.225, 0.435)
fac-OCF$_3$	461, 492	454, 487, 525	(0.197, 0.315)	(0.173, 0.240)
fac-F	453, 482	446, 477, 509	(0.193, 0.289)	(0.172, 0.214)
CF$_3$acac	498, 531	492, 530, 572	(0.282, 0.531)	(0.256, 0.505)
OCF$_3$acac	473, 503	466, 501, 539	(0.286, 0.434)	(0.197, 0.330)
Facac	539	455, 488, 523	(0.356, 0.435)	(0.215, 0.316)
OCH$_3$acac	540	458, 491, 527	(0.426, 0.471)	(0.281, 0.404)
Hacac	485, 516, 542	472, 506, 545	(0.508, 0.491)	(0.211, 0.363)
MHacac	474, 512, 539	470, 504, 542	(0.371, 0.457)	(0.221, 0.353)
FIrpic	472		(0.174, 0.308)	

dx.doi.org/10.1021/ic400950u | *Inorg. Chem.* XXXX, XXX, XXX−XXX

Table 7. Phosphorescence Quantum Yields and Lifetimes Measured in 2-MeTHF

	Φ_{PL} (298 K]	Φ_{PL} (77 K)	τ [ns]	k_r [10^5 s^{-1}]	k_{nr} [10^5 s^{-1}]
fac-CF_3	0.40	0.41	2.81×10^3	1.4	2.1
fac-OCF_3	0.53	0.56	3.32×10^3	1.6	1.4
fac-F	0.60	not measured	3.36×10^3	1.7	1.2
CF_3acac	0.28	0.34	2.46×10^3	1.1	2.9
OCF_3acac	0.0079	0.47	76.9 (96.6%), 0.960 (3.4%)	0.95	1.3×10^2
Facac	0.0037	0.40	33.5 (82.5%), 257 (17.5%)	1.1	3.0×10^2
OCH_3acac	0.0024	0.11	28.8 (48.8%), 0.465 (51.2%)	0.87	3.5×10^2
Hacac	0.0022	0.32	25.6 (89.7%), 1.01 (10.3%)	0.63	3.9×10^2
MHacac	0.0026	0.28	24.1 (48.9%), 0.463 (51.1%)	1.2	4.1×10^2

emissions of imidazolyl diketonate complexes have been reported to show strong solvent dependence.[26]

However, a clear vibrational structure appeared at 77 K, and all complexes showed efficient blue to green phosphorescence ($\Phi_{PL} > 0.11$). Observation of the emission 0,0 band in a glassy matrix at 77 K assists understanding of the substituent effect on the emission λ_{max}. For example, λ_{max} for CF_3acac was red-shifted by 20 nm (472−492 nm, 860 cm^{-1}) relative to that of Hacac. However, *fac*-Ir(ppy)$_3$, which has small LUMO localization on the phenyl moiety, had λ_{max} = 494 nm with no spectral shift by trifluoromethyl substitution at 77 K.[29] DFT calculations showed that the imidazolinate complexes studied here have similar MO character with *fac*-Ir(ptz)$_3$ reported by Samuel, which exhibited a 13 nm (449−462 nm, 620 cm^{-1}) red-shift by trifluoromethyl substitution at 298 K.[23] The red-shift of the imidazolinate complexes and *fac*-Ir(ptz)$_3$ by trifluoromethyl substitution, where the LUMO is localized on the phenyl moiety more than the HOMO, reveals the stabilization of the LUMO. Comparison of the Swain−Lupton constants in Table 4 and λ_{max} shows that the trifluoromethyl group has an *F* value 0.35 higher than that of H, which indicates the stronger electron withdrawing effect. Complexes of OCF_3acac, Facac, and OCH_3acac (except CF_3acac) had λ_{max} between 455 and 466 nm, which were blue-shifted compared with that for Hacac at λ_{max} = 472 nm. In particular, OCF_3acac had λ_{max} = 466 nm that was 26 nm (1130 cm^{-1}) shorter than that of CF_3acac (492 nm). The *F* value of the trifluoromethoxy group is almost the same as that of the trifluoromethyl group; however, the former has an *R* value that is 0.20 smaller than that of latter. This resonance effect destabilizes LUMO, and *R* values are even smaller for the fluoro and methoxy groups; therefore, destabilization of the LUMO gives a larger HOMO−LUMO energy gap.

Substitution on the phenyl moiety with electron-donating substituents is effective to obtain blue-shifted emissions. Hacac and MHacac gave identical λ_{max}; however, Hacac gave an *x* CIE chromaticity coordinate that was 0.01 smaller than that of MHacac. *N*-Butyl substitution caused a slight blue-shift than that for *N*-methyl substitution (Figure 5 and Table 6).

As discussed in the DFT section, section 3.2, substitution has a significant effect on the emission quantum efficiency. This can be explained from the energy difference (ΔE) between the LUMO and MO localized on the acetylacetone moiety. Table 2 shows the percentage MO (LUMO to LUMO + 2) contribution of iridium metal (Ir), phenyl (Ph), imidazolyl (Im), and acetylacetonate (acac) moieties, and the MO energy levels (*E*) calculated by the DFT method. For example, in the case of CF_3acac, ΔE is 0.49 eV ($E_{LUMO} - E_{LUMO+2}$ = 1.54−1.05), and for OCF_3acac, ΔE is 0.22 eV ($E_{LUMO} - E_{LUMO+2}$ = 1.25−1.03). ΔE is plotted as function of the logarithm of Φ_{PL} at 298 K (Figure 6). When the LUMO was localized on acetylacetone (OCH_3acac and Hacac), ΔE is treated as zero.

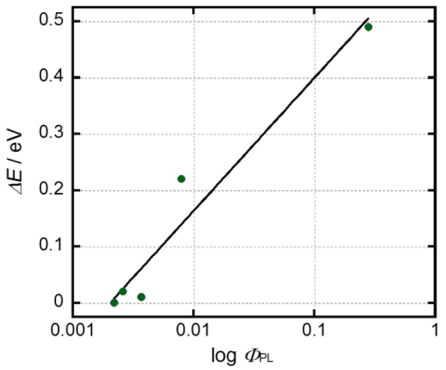

Figure 6. Plot of ΔE versus log Φ_{PL}.

This plot indicates that a larger ΔE gives a larger Φ_{PL}; therefore, simple MO energy levels calculated for optimized structure are useful to understand nonradiative deactivation processes through the ancillary ligand. The weak and broad emission of CF_3acac and OCF_3acac at 298 K is caused by the quenching of excitation energy by the acetylacetone part. The inefficiencies of other diketonated complexes at 298 K are due to thermal activation to the upper excited state responsible for nonradiative deactivation. Therefore, these thermal activations are prohibited at 77 K. The smallest Φ_{PL} of OCH_3acac among the diketonate complexes at 77 K is explained by the LUMO being localized on acetylacetone.

In contrast, the homoleptic complexes showed efficient emission, not only at 77 K, but also at 298 K (Φ_{PL} = 0.40−0.60). Phosphorescence spectra of homoleptic complexes are shown in Figure 7. No significant difference of k_r between the homoleptic and diketonate complexes was evident, whereas k_{nr} become smaller for the homoleptic complexes than for the diketonate complexes. For example, in the case of *fac*-F and Facac, k_r is almost the same (1.1 and 1.7 × 10^5 s^{-1}); however, k_{nr} decreased by almost 1/300.

A blue-shift of λ_{max} was observed for the homoleptic complexes compared with those of the corresponding diketonate complexes. For example, λ_{max} values of CF_3acac and *fac*-CF_3 were 492 and 483 nm at 77 K, respectively. Similar blue-shifts of 8 nm (395 cm^{-1}) were also observed for *fac*-OCF_3 and *fac*-F. In particular, that for *fac*-F (λ_{max} = 453 nm) is shorter than that for FIr6 (λ_{max} = 458 nm[47]), which has one of the shortest λ_{max} of the phenylpyridinate complexes. The CIE chromaticity coordinates (0.193, 0.289) were also equivalent to those of FIr6 (0.16, 0.27).[48] *fac*-OCF_3 also had good coordinates (0.197, 0.315) that are equivalent to those of

dx.doi.org/10.1021/ic400950u | Inorg. Chem. XXXX, XXX, XXX−XXX

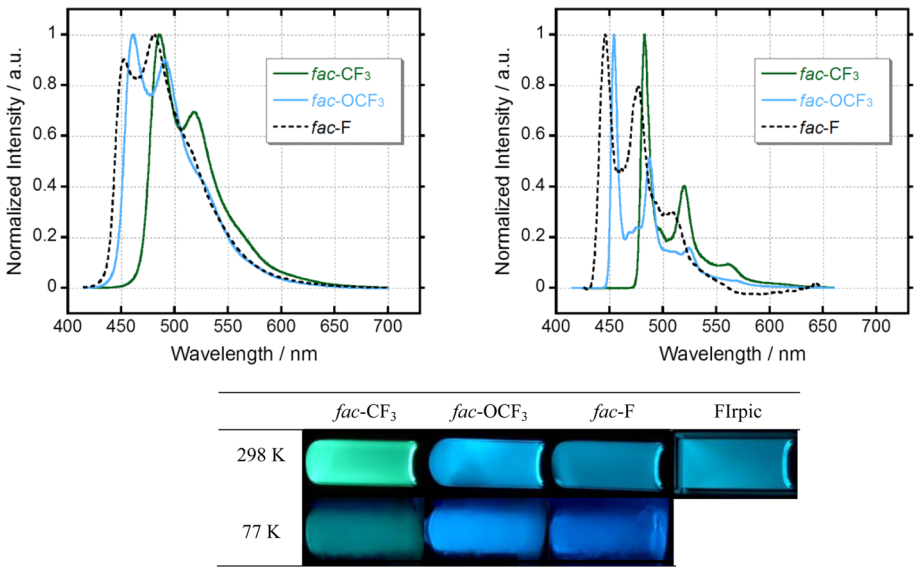

Figure 7. Phosphorescence spectra for homoleptic complexes measured in 2-MeTHF (at 298 K) and in a glassy matrix (at 77 K). Photographs of phosphorescence of homoleptic complexes measured in 2-MeTHF (at 298 K) and in a glassy matrix (at 77 K).

FIrpic (0.17, 0.34).[49] *fac*-CF_3 has low solubility; however, *fac*-OCF_3 has much better solubility in organic solvents. All of the homoleptic complexes had emission lifetimes (2.81−3.36 μs) suitable for device fabrication.

3.6. Temperature Dependence of Emission Lifetime. Figure 8 and Table S3 in the Supporting Information show the

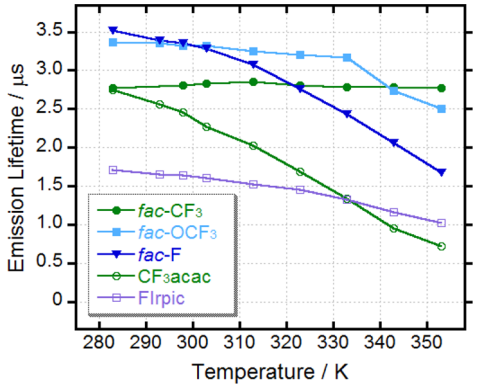

Figure 8. Temperature dependence of emission lifetime measured in 2-MeTHF.

effect of temperature on the emission intensity and lifetime for *fac*-CF_3, *fac*-OCF_3, *fac*-F, CF_3acac, and FIrpic between 283 and 353 K. In case of CF_3acac, the lifetime at 298 K (2.46 μs) was decreased 71% by increasing the temperature to 353 K (0.714 μs). This is caused by thermal activation of the nonradiative deactivation process through the acetylacetone moiety. However, almost no change was observed for *fac*-CF_3 (2.81 μs at 298 K and 2.77 μs at 353 K). In the case of *fac*-OCF_3, lifetime decreased from 3.32 to 2.50 μs (25%) by increase of the temperature from 298 to 353 K. The slope of the plot may be larger for temperatures higher than 333 K. In the case of *fac*-F, the lifetime was decreased 50%, from 3.36 μs (298 K) to 1.68 μs (353 K), by increase in the temperature. The frontier orbital energy calculated by the DFT method is shown in Figure 9, which indicates that the LUMO energy level is in the order of *fac*-CF_3 < *fac*-OCF_3 < *fac*-F. In a comparison of this with the

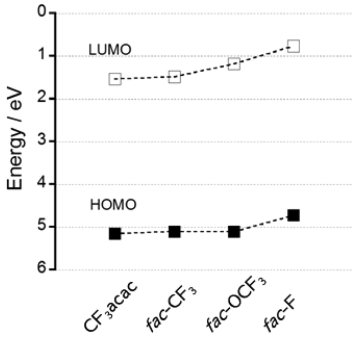

Figure 9. HOMO and LUMO energy levels calculated by the DFT method (RB3LYP/LANL2DZ).

lifetime temperature dependence, a higher LUMO position effectively decreases the emission lifetime. This is explained by a thermal equilibrium between the state responsible for the emission and the d* state responsible for nonradiative deactivation. This phenomenon of phenylimidazolynato complexes is similar to that observed for phenylpyridinato and phenylpyrazolynato complexes as reported by Thompson and co-workers.[50]

3.7. OLED Device. OLED devices were fabricated for *fac*-OCF_3, which showed efficient luminescence in 2-MeTHF, and FIrpic was used as a reference. Figure 10 shows the device configuration. The wet-processable *m*-terphenyl derivative, 3,3″,5,5″-tetra(9*H*-carbazol-9-yl)-1,1′:3′,1″-terphenyl (mB-4Cz), was synthesized as a host material.[51] The HOMO−LUMO energy levels are also indicated in the figure. The reported HOMO energy level for FIrpic was obtained by CV, and the HOMO−LUMO energy gap was determined by the 0−0 band (468 nm) in CH_2Cl_2 at 298 K.[52] In this study, a similar method was applied to determine the HOMO−LUMO energy levels of *fac*-OCF_3.

The performances of the fabricated devices were determined from plots of current density (J, mA/cm^2), luminance (L, cd/m^2), and current efficiency (η, cd/A) versus applied voltage (V, V), as shown in Figure 11 and summarized in Table 8.

dx.doi.org/10.1021/ic400950u | Inorg. Chem. XXXX, XXX, XXX−XXX

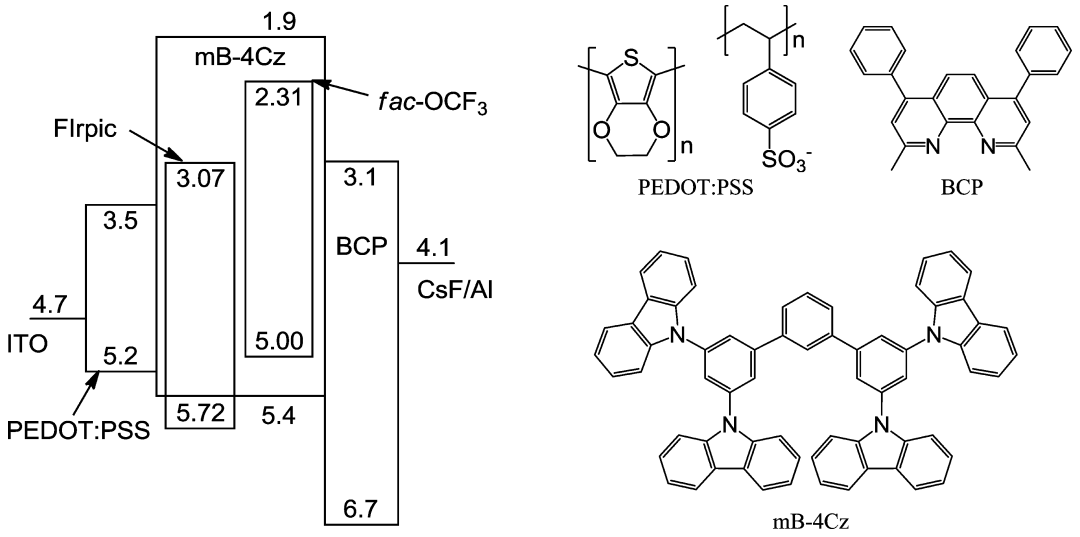

Figure 10. Device structure and energy diagram[51,52] (left, units in eV) and chemical structures of the materials (right).

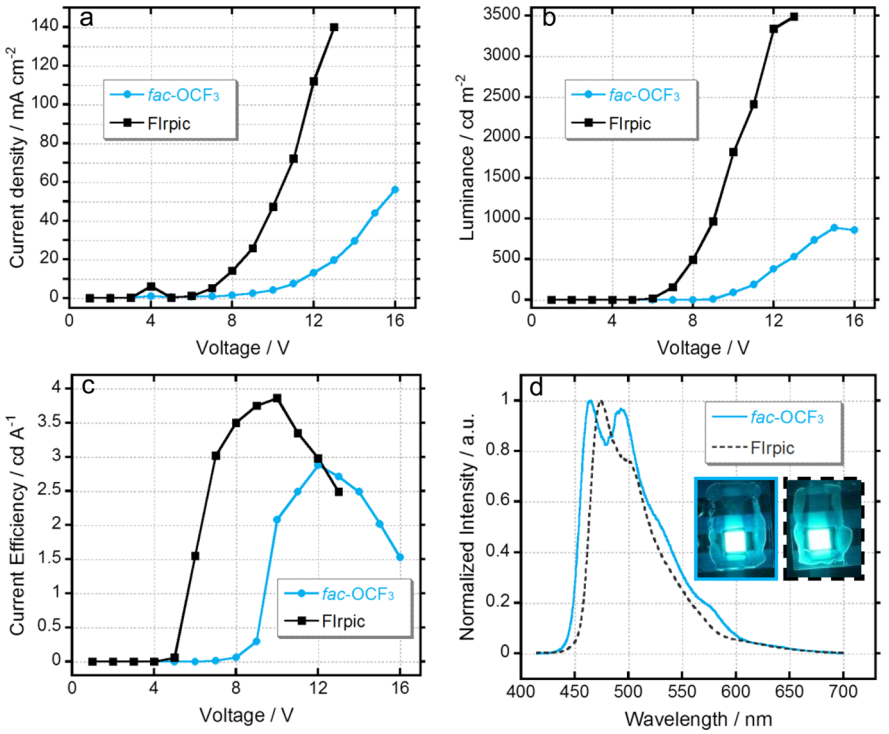

Figure 11. (a) *J*–*V*, (b) *L*–*V*, and (c) η–*V* characteristics. (d) EL spectra and photographs of the fabricated devices.

Table 8. Emission Characteristics for the OLED Devices Measured in 2-MeTHF

		λ_{max} [nm]	CIE (*x*, *y*)	L_{max} [cd/m^2]	η_{max} [cd/A], (*J*) [mA/cm^2]
fac-OCF_3	device	464, 494	(0.232, 0.354)	889 (15 V)	2.88 (13.2)
	solution	461, 491	(0.197, 0.315)		
FIrpic	device	474	(0.200, 0.345)	3490 (13 V)	3.86 (47.2)
	solution	472	(0.174, 0.308)		

EL spectra of both devices were red-shifted by 2–3 nm (140 and 89 cm^{-1} for *fac*-OCF_3 and FIrpic, respectively) and had smaller 0–0 bands than the 0–1 band, compared with the spectra measured in 2-MeTHF (Figure 7). Therefore, the CIE coordinates (*x* and *y*) were slightly increased. The coordinate of FIrpic is more blue than that of *fac*-OCF_3; however, there was no significant difference observed by visual check.

The maximum luminance for *fac*-OCF_3 and FIrpic was 889 and 3490 cd/m^2, respectively. The lower luminance of *fac*-OCF_3 is explained by inefficient carrier injection into the emitting layer. This is supported by both the inefficient current density and larger driving voltage. The HOMO–LUMO energy levels of *fac*-OCF_3 were shifted by approximately 0.7 eV to higher energy than those for FIrpic (Figure 10).

From the energy diagram in Figure 10, the HOMO–LUMO level of *fac*-OCF_3 is moved by 0.7 V almost parallel to those of FIrpic in the anodic direction. Therefore, charge injection from

dx.doi.org/10.1021/ic400950u | Inorg. Chem. XXXX, XXX, XXX–XXX

the charge conducting layer to the emitting layer became difficult in the case of *fac*-OCF_3. The HOMO level of *fac*-OCF_3 is higher than that of PEDOT:PSS. The HOMO−LUMO energy levels of imidazole have been reported to take high values among some nitrogen-containing cyclic compounds, according to *ab initio* calculations.[46]

The FIrpic device has the same configuration with the mB-4Cz host materials. A hole only device (device fabricated without a PEDOT:PSS layer) and an electron only device (device fabricated with no BCP layer) were fabricated, and the *J*−*V* characteristics were measured. The hole and electron only devices showed current densities of 237 and 64 mA/cm^2, respectively, at an applied voltage of 10 V.[42] Therefore, the high hole and low electron transferability of mB-4Cz is partly responsible for the moderate performance of these devices.

4. CONCLUSIONS

Homoleptic and heteroleptic acetylacetonato phenylimidazolinato Ir(III) complexes with various substituents were synthesized. X-ray crystallographic analyses of single crystals of *fac*-CF_3 and *fac*-OCF_3 showed their octahedral structures.

DFT calculations of all complexes revealed the HOMO delocalized on the d-orbital of iridium and the phenyl moiety, similar to that of *fac*-Ir(ppy)$_3$. The LUMO of *fac*-Ir(ppy)$_3$ is localized at the pyridyl moiety; however, the LUMO of imidazolinato complexes is localized at the phenyl moiety to a greater extent than the HOMO.

These complexes had reversible oxidation voltammograms, and the HOMO was destabilized by approximately 0.2−0.5 eV, relative to those of phenylpyridinato, phenylpyrazolinato, phenylimidazolinato-carbene type, and phenyltriazolinato iridium(III) complexes.

Substitution on phenyl ring with trifluoromethyl groups induced a red-shift of phosphorescence, and a blue-shift was observed for other substituents, such as fluoro, methoxy, and trifluoromethoxy groups. Therefore, π-electron donating substituents (resonance effect) can induce a blue-shift of the emission spectra. This is explained by the DFT results that indicate localization of the LUMO on the phenyl moiety is more significant than that for the HOMO. Diketonate complexes with green phosphorescence gave efficient emission; however, the blue phosphorescence complexes showed poor efficiency. This is due to the shift of the emissive LUMO energy level toward higher energy, which resulted in a decrease in the energy difference between the LUMO and MO localized on the diketonate ligand.

The effect of temperature on the lifetime indicates blue-shift of emission spectra has a correlation with the shortening of the emission lifetime at high temperature.

OLED devices fabricated using *fac*-OCF_3 or FIrpic as a dopant showed similar emission colors. Emission luminance of the former was smaller than that of the latter. This may be due to the higher HOMO and LUMO (by 0.7 eV) of *fac*-OCF_3 than that of FIrpic, which prevents charge injection from the charge conducting layer to the emissive layer.

■ ASSOCIATED CONTENT

Ⓢ Supporting Information

Crystallographic data in CIF format. ^{1}H NMR, ESI-MS, CV, time-correlated single photon counting decay profiles, and EL spectra of complexes. These materials are available free of charge via the Internet at http://pubs.acs.org.

■ AUTHOR INFORMATION

Corresponding Author

*E-mail: karatsu@faculty.chiba-u.jp (T.K.). Fax: +81-43-290-3401.

Notes

The authors declare no competing financial interest.

■ ACKNOWLEDGMENTS

The authors thank Dr. Koichi Ishibashi and Ms. Kyoko Endo (Mitsubishi Chemical Corporation-Group Science and Technology Research Center) for stimulating discussions; Professor Hyuma Masu, Professor Masami Sakamoto, and Dr. Fumitoshi Yagishita (Analytical Center, Chiba University) for support with single crystal X-ray crystallography; Professor Norihisa Kobayashi and Mr. Naoki Ura (Department of Image Sciences, Chiba University) for measurement of CV; and Dr. Lin Xu (Department of Applied Chemistry and Biotechnology, Chiba University) for fabrication of the OLEDs. The authors thank the Analytical Center of Chiba University for help with the materials analyses. This work was supported by a Grant-in-Aid for Scientific Research (20550056) and the G-COE program (Advanced School for Organic Electronics) from the Ministry of Education, Culture, Sports, Science and Technology (MEXT) of Japan.

■ REFERENCES

(1) *Highly Efficient OLEDs with Phosphorescent Materials*; Yersin, H., Ed.; Wiley VCH: Berlin, Germany, 2007.
(2) Tanaka, D.; Sasabe, H.; Li, Y.-J.; Su, S.-J.; Takeda, T.; Kido, J. *Jpn. J. Appl. Phys.* **2007**, *46*, L10−12.
(3) Tang, C. W.; Vanslyke, S. A. *Appl. Phys. Lett.* **1987**, *51*, 913−915.
(4) Baldo, M. A.; O'Brien, D. F.; You, Y.; Shoustikov, A.; Sibley, S.; Thompson, M. E.; Forrest, S. R. *Nature* **1998**, *395*, 151−154.
(5) Baldo, M. A.; Lamansky, S.; Burrows, P. E.; Thompson, M. E.; Forrest, S. R. *Appl. Phys. Lett.* **1999**, *75*, 4−6.
(6) Xiao, L.; Chen, Z.; Qu, B.; Luo, J.; Kong, S.; Gong, Q.; Kido, J. *Adv. Mater.* **2011**, *23*, 926−952.
(7) Adachi, C.; Kwong, R. C.; Djurovich, P.; Adamovich, V.; Baldo, M. A.; Thompson, M. E.; Forrest, S. R. *Appl. Phys. Lett.* **2001**, *79*, 2082−2084.
(8) Holmes, R. J.; D'Andrade, B. W.; Forrest, S. R.; Ren, X.; Li, J.; Thompson, M. E. *Appl. Phys. Lett.* **2003**, *83*, 3818.
(9) Yeh, S.-J.; Wu, M.-F.; Chen, C.-T.; Song, Y.-H.; Chi, Y.; Ho, M.-H.; Hsu, S.-F.; Chen, C. H. *Adv. Mater.* **2005**, *17*, 285−289.
(10) Tamayo, A. B.; Alleyne, B. D.; Djurovich, P. I.; Lamansky, S.; Tsyba, I.; Ho, N. N.; Bau, R.; Thompson, M. E. *J. Am. Chem. Soc.* **2003**, *125*, 7377−7387.
(11) Sajoto, T.; Djurovich, P. I.; Tamayo, A.; Yousufuddin, M.; Bau, R.; Thompson, M. E.; Holmes, R. J.; Forrest, S. R. *Inorg. Chem.* **2005**, *44*, 7992−8003.
(12) Ragni, R.; Plummer, E. A.; Brunner, K.; Hofstraat, J. W.; Babudri, F.; Farinola, G. M.; Naso, F.; De Cola, L. *J. Mater. Chem.* **2006**, *16*, 1161−1170.
(13) Sivasubramaniam, V.; Brodkorb, F.; Hanning, S.; Loebl, H. P.; van Elsbergen, V.; Boerner, H.; Scherf, U.; Kreyenschmidt, M. *J. Fluorine Chem.* **2009**, *130*, 640−649.
(14) Lin, C.-H.; Chang, Y.-Y.; Hung, J.-Y.; Lin, C.-Y.; Chi, Y.; Chung, M.-W.; Lin, C.-L.; Chou, P.-T.; Lee, G.-H.; Chang, C.-H.; Lin, W.-C. *Angew. Chem., Int. Ed.* **2011**, *50*, 3182−3186.
(15) Lamansky, S.; Djurovich, P.; Murphy, D.; Abdel-Razzaq, F.; Kwong, R.; Tsyba, I.; Bortz, M.; Mui, B.; Bau, R.; Thompson, M. E. *Inorg. Chem.* **2001**, *40*, 1704−1711.
(16) Lamansky, S.; Djurovich, P.; Murphy, D.; Abdel-Razzaq, F.; Lee, H.-E.; Adachi, C.; Burrows, P. E.; Forrest, S. R.; Thompson, M. E. *J. Am. Chem. Soc.* **2001**, *123*, 4304−4312.

(17) Coppo, P.; Plummerab, E. A.; De Cola, L. *Chem. Commun.* **2004**, 1774−1775.
(18) Yang, C.-H.; Cheng, Y.-M.; Chi, Y.; Hsu, C.-J.; Fang, F.-C.; Wong, K.-T.; Chou, P.-T.; Chang, C.-H.; Tsai, M.-H.; Wu, C.-C. *Angew. Chem., Int. Ed.* **2007**, *46*, 2418−2421.
(19) Chiu, Y.-C.; Lin, C.-H.; Hung, J.-Y.; Chi, Y.; Cheng, Y.-M.; Wang, K.-W.; Chung, M.-W.; Lee, G.-H.; Chou, P.-T. *Inorg. Chem.* **2009**, *48*, 8164−8172.
(20) Hung, J.-Y.; Chi, Y.; Pai, I.-H.; Yu, Y.-C.; Lee, G.-H.; Chou, P.-T.; Wong, K.-T.; Chenc, C.-C.; Wu, C.-C. *Dalton Trans.* **2009**, 6472−6475.
(21) Holmes, R. J.; Forrest, S. R.; Sajoto, T.; Tamayo, A.; Djurovich, P. I.; Thompson, M. E.; Brooks, J.; Tung, Y.-J.; D'Andrade, B. W.; Weaver, M. S.; Kwong, R. C.; Brown, J. J. *Appl. Phys. Lett.* **2005**, *87*, 243507.
(22) Tsuchiya, K.; Yagai, S.; Kitamura, A.; Karatsu, T.; Endo, K.; Mizukami, J.; Akiyama, S.; Yabe, M. *Eur. J. Inorg. Chem.* **2010**, 926−933.
(23) Lo, S.-C.; Shipley, C. P.; Bera, R. N.; Harding, R. E.; Cowley, A. R.; Burn, P. L.; Samuel, I. D. W. *Chem. Mater.* **2006**, *18*, 5119−5129.
(24) Bolink, H. J.; De Angelis, F.; Baranoff, E.; Klein, C.; Fantacci, S.; Coronado, E.; Sessolo, M.; Kalyanasundaram, K.; Grätzel, M.; Nazeeruddin, M. K. *Chem. Commun.* **2009**, 4672−4674.
(25) Baranoff, E.; Fantacci, S.; De Angelis, F.; Zhang, X.; Scopelliti, R.; Grätzel, M.; Nazeeruddin, M. K. *Inorg. Chem.* **2011**, *50*, 451−462.
(26) Jayabharathi, J.; Thanikachalam, V.; Srinivasan, N.; Perumal, M. V. *J. Fluoresc.* **2011**, *21*, 1585−1597.
(27) Ouk, S.; Thiébaud, S.; Borredon, E. *Synth. Commun.* **2005**, *35*, 3021−3026.
(28) Heravi, M. M.; Derikvand, F.; Haghighi, M. *Monatsh. Chem.* **2008**, *139*, 31−33.
(29) Dedeian, K.; Djurovich, P. I.; Garces, F. O.; Carlson, C.; Watts, R. J. *Inorg. Chem.* **1991**, *30*, 1685−1687.
(30) Nonoyama, M. *Bull. Chem. Soc. Jpn.* **1974**, *47*, 767−768.
(31) Farrugia, L. J. *J. Appl. Crystallogr.* **1997**, *30*, 565.
(32) Momma, K.; Izumi, F. *J. Appl. Crystallogr.* **2011**, *44*, 1272−1276.
(33) Ashraf, R. S.; Shahid, M.; Klemm, E.; Al-Ibrahim, M.; Sensfuss, S. *Macromol. Rapid Commun.* **2006**, *27*, 1454−1459.
(34) Demas, J. N.; Crosby, G. A. *J. Phys. Chem.* **1971**, *75*, 991−1024.
(35) Murov, S. L.; Carmichael, I.; Hug, G. L., *Handbook of Photochemistry*, 2nd ed.; Marcel Dekker: New York, 1993.
(36) Karatsu, T.; Ito, E.; Yagai, S.; Kitamura, A. *Chem. Phys. Lett.* **2006**, *424*, 353−537.
(37) Kobe, K. A.; Ravicz, A. E.; Vohra, S. P. *J. Chem. Eng. Data* **1956**, *1*, 50−56.
(38) Frisch, M. J.; Trucks, F. W.; Schlegel, H. B.; Scuseria, G. E.; Robb, M. A.; Cheeseman, J. R.; Montgomery, J. A., Jr.; Vreven, T.; Kudin, K. N.; Burant, J. C.; Millam, J. M.; Iyengar, S. S.; Tomasi, J.; Barone, V.; Mennucci, B.; Cossi, M.; Scalmani, G.; Rega, N.; Petersson, G. A.; Nakatsuji, H.; Hada, M.; Ehara, M.; Toyota, K.; Fukuda, R.; Hasegawa, J.; Ishida, M.; Nakajima, T.; Honda, Y.; Kitao, O.; Nakai, H.; Klene, M.; Li, X.; Knox, J. E.; Hratchian, H. P.; Cross, J. B.; Bakken, V.; Adamo, C.; Jaramillo, J.; Gomperts, R.; Stratmann, R. E.; Yazyev, O.; Austin, A. J.; Cammi, R.; Pomelli, C.; Ochterski, J. W.; Ayala, P. Y.; Morokuma, K.; Voth, G. A.; Salvador, P.; Dannenberg, J. J.; Zakrzewski, V. G.; Dapprich, S.; Daniels, A. D.; Strain, M. C.; Farkas, O.; Malick, D. K.; Rabuck, A. D.; Raghavachari, K.; Foresman, J. B.; Ortiz, J. V.; Cui, Q.; Baboul, A. G.; Clifford, S.; Cioslowski, J.; Stefanov, B. B.; Liu, G.; Liashenko, A.; Piskorz, P.; Komaromi, I.; Martin, R. L.; Fox, D. J.; Keith, T.; Al-Laham, M. A.; Peng, C. Y.; Nanayakkara, N.; Challacombe, M.; Gill, P. M. W.; Johnson, B.; Chen, W.; Wong, M. W.; Gonzalez, C.; Pople, J. A. *Gaussian 03, revision C.01*; Gaussian, Inc.: Wallingford, CT, 2004.
(39) Becke, A. D. *J. Chem. Phys.* **1993**, *98*, 5648−5652.
(40) Hay, P. J. *J. Phys. Chem. A* **2002**, *106*, 1634−1641.
(41) O'Boyle, N. M.; Tenderholt, A. L.; Langner, K. M. *J. Comput. Chem.* **2008**, *29*, 839−845.
(42) Hattori, T. *Master Thesis*, Chiba University, 2012.
(43) Treboux, G.; Mizukami, J.; Yabe, M.; Nakamura, S. *J. Photopolym. Sci. Technol.* **2008**, *21*, 347−348.
(44) Fei, T.; Gu, X.; Zhang, M.; Wang, C.; Hanif, M.; Zhang, H.; Ma, Y. *Synth. Met.* **2009**, *159*, 113−118.
(45) Hansch, C.; Leo, A.; Taft, R. W. *Chem. Rev.* **1991**, *91*, 165−195.
(46) Tamao, K.; Uchida, M.; Izumizawa, T.; Furukawa, K.; Yamaguchi, S. *J. Am. Chem. Soc.* **1996**, *118*, 11974−11975.
(47) Endo, A.; Suzuki, K.; Yoshihara, T.; Tobita, S.; Yahiro, M.; Adachi, C. *Chem. Phys. Lett.* **2008**, *460*, 155−157.
(48) Zheng, Y.; Eom, S.-H.; Chopra, N.; Lee, J.; So, F.; Xuea, J. *Appl. Phys. Lett.* **2008**, *92*, 223301.
(49) Tokito, S.; Iijima, T.; Suzuri, Y.; Kita, H.; Tsuzuki, T.; Sato, F. *Appl. Phys. Lett.* **2003**, *83*, 569−571.
(50) Sajoto, T.; Djurovich, P. I.; Tamayo, A. B.; Oxgaard, J.; Goddard, W. A., III; Thompson, M. E. *J. Am. Chem. Soc.* **2009**, *131*, 9813−9822.
(51) Lin, X.; Yagai, S.; Kitamura, A.; Hwang, D.-R.; Park, S.-Y.; Park, Y.-S.; Kim, J.-J.; Karatsu, T. *Synth. Met.* **2012**, *162*, 303−308.
(52) Baranoff, E.; Curchod, B. F. E.; Monti, F.; Steimer, F.; Accorsi, G.; Tavernelli, I.; Rothlisberger, U.; Scopelliti, R.; Grätzel, M.; Nazeeruddin, M. K. *Inorg. Chem.* **2012**, *51*, 799−811.